J Mater Sci (2007) 42:4205–4214
DOI 10.1007/s10853-006-0644-0

Intermetallic Fe_xAl_y-phases in a steel/Al-alloy fusion weld

Leonardo Agudo · Dominique Eyidi · Christian H. Schmaranzer · Enno Arenholz · Nasrin Jank · Jürgen Bruckner · Anke R. Pyzalla

Received: 24 May 2006 / Accepted: 5 July 2006 / Published online: 2 March 2007

Abstract The microstructure of joints between an Al-alloy and a zinc coated ferritic steel sheet manufactured by the so-called CMT joining method is investigated. The joint consists of a weld between the Al-alloy and Al 99.8 filler and a brazing of the filler to the zinc coated steel. The morphology, the structure and the defects of the intermetallic phases that developed at the interface between the steel and the Al 99.8 filler are characterised using scanning and transmission electron microscopy. The intermetallic phase seam is only about 2.3 μm thick and consists of trapezoidal nearly equiaxial Fe_2Al_5 grains surrounded by finger-like remains of the steel and mostly elliptical $FeAl_3$ grains extending into the Al 99.8 filler material. Both the Fe_2Al_5 and the $FeAl_3$ grains contain crystal defects.

L. Agudo (✉) · N. Jank · A. R. Pyzalla
TU Wien, Institute of Material Science and Technology, Karlsplatz 13-308, 1040 Vienna, Austria
e-mail: agudo@mpie.de

Present Address:
L. Agudo · A. R. Pyzalla
Max-Planck-Institute for Iron Research GmbH, Max-Planck-Str. 1, 40237 Düsseldorf, Germany

D. Eyidi
TU Wien, University Service for Transmission Electron Microscopy, Wiedner Haupstrasse 8-10, 1040 Vienna, Austria

Present Address:
D. Eyidi
Laboratoire de Métallurgie Physique UMR 6630 CNRS–Université de Poitiers, SP2MI, BP 30179, 86962 Chasseneuil Futuroscope Cedex, France

C. H. Schmaranzer · E. Arenholz
Voestalpine Stahl GmbH, Voestalpine-Straße 3, 4020 Linz, Austria

N. Jank · J. Bruckner
Fronius International, Sparte Schweißtechnik, Buxbaumstrasse 2, 4600 Wels, Austria

Introduction

The necessity for lightweight constructions in automotive and other transportation industry has produced a strong interest in the joining of steels to Al-alloys. Today, most steel/Al-alloy joints are either form-fit or force-fit joints, which is due to the difficulties in substance-to-substance bonding arising mainly from the differences in the melting points of steel and Al-alloys, the differences in their thermal conductivity, the extremely low solubility of Fe in Al and due to the formation of intermetallic Fe_xAl_y-phases (Fig. 1) [1]. The formation of Fe_xAl_y-phases is necessary for achieving an effectual connection between the steel and the Al-alloys. However, an excessive formation of intermetallic Fe_xAl_y-phases, in particular of Al-rich Fe_xAl_y-phases, results in brittleness of the joints.

The intermetallic Fe_xAl_y-phases form both due to chemical reactions and due to interdiffusion between Fe and Al. Concepts for limiting the amount of Fe_xAl_y-phases in steel to Al-alloys substance-to-substance bonding attempt to inhibit the chemical reaction between Fe and Al or to obstruct the interdiffusion between Fe and Al.

One option to limit the heat in the joint and, therefore, the intensity of chemical reactions and

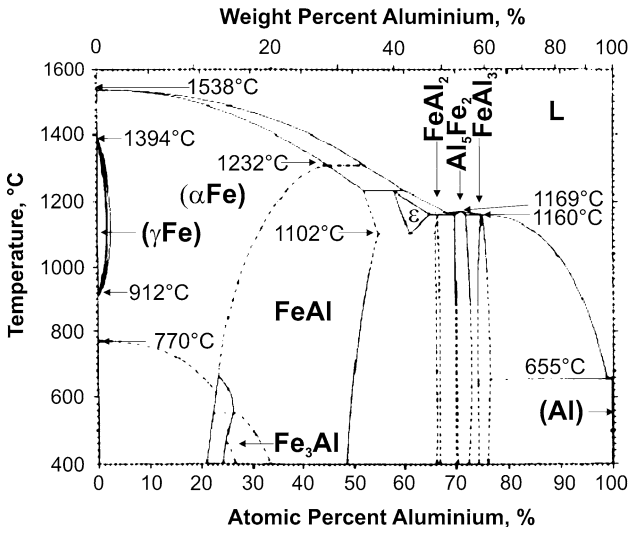

Fig. 1 The Fe–Al phase diagram [1]

diffusion is the use of pressure welding techniques e.g. diffusion welding [2, 3], explosion welding [4], friction welding [4, 5] and the comparatively new friction stir welding technique [6, 7].

Due to the large difference in the melting points between steels and Al-alloys, in case of fusion welding these two materials, the Al-alloy usually melts while the steel remains in solid state. Thus, joining of Al-alloy to steel is usually achieved via filler, where the Al-alloy is welded to the filler material while brazing occurs between the filler and the steel. The formation and growth of the intermetallic phases between the liquid filler and the solid steel is governed both by chemical reaction and by interdiffusion.

Early strategies to limit reaction and interdiffusion between Fe and Al consisted in buffering the steel, e.g. with layers mainly of Ag, Ni or Cu [4, 8, 9] and in tungsten inert gas (TIG) welding respectively brazing using AlSi5 fillers. Currently also the possibility for laser joining of steel to Al-alloys is explored [3, 10].

We used a new metal inert gas welding technique developed for welds with lower heat input. The aim of this study is the characterisation of the microstructure of the joint and in particular the identification of the intermetallic phases that form between the filler and the steel sheet. The intermetallic phase seam in the cold metal transfer (CMT) welds is substantially thinner than in case of pressure-welded joints and hot dip aluminised steel, thus, we concentrate here on transmission electron microscopy.

Details about the mechanical properties of the welds, their residual stress state and their formability in subsequent manufacturing processes are given in [11, 12].

Experimental details

Welding procedure

The welds were manufactured at Fronius International GmbH, Wels, Austria using the so-called ''Cold Metal Transfer'' method for automated metal inert gas welding. The main characteristic that distinguishes the CMT welding process from conventional metal inert gas welding is the incorporation of the wire motion into process-control. The wire is moved forward and backward—once short circuit has happened—with a frequency of up to 70 Hz. The wire retraction assists droplet detachment and thus a current-free material transfer. Due to the current-free material transfer and the discontinuation of the short circuit the heat input during the welding process is substantially reduced compared to conventional metal arc welding and it is virtually splatter-free [13].

The steel/Al-alloy joints investigated are overlap welds of a 1 mm thick A6061 T4 plate to DX56D steel coated with Zn Z140 (~10 μm thick zinc layer), provided by Voestalpine Stahl GmbH, using an Al 99.8 filler. The parameters of the welding process are $I = 70$ A, $U = 12$ V, $v = 60$ cm/min in Ar 4.6 atmosphere.

Metallography, optical and scanning electron microscopy

For optical and scanning electron microscopy cross-sections of the samples were cut, grinded, polished and inspected for cracks and pores in the intermetallic layer. Other samples were etched in nital in order to reveal the grain boundaries of the steel and visualize the intermetallic Fe_xAl_y-phases. A Phillips XL30 scanning electron microscope, equipped with an EDAX energy dispersive X-ray (EDX) elemental analyser, was employed to perform the scanning electron microscopy (SEM) studies.

Transmission electron microscopy

Specimens were prepared from weld cross-sections by mechanical grinding and polishing them down to a thickness of 30 μm. Afterwards, the samples were ion milled to target the intermetallic layer. Transmission electron microscopy (TEM) was performed using an analytical 200 kV FEG-TEM TECNAI F20 S-Twin TEM equipped with an EDX detector and a Gatan imaging filter. Conventional Dark-Field (DF), bright-field (BF), selected area diffraction and high-angle annular dark-field (Z-contrast) techniques were used

to investigate the microstructure. Diffraction patterns were simulated using the EMS program available online [14]. All EDX spectra were recorded in scanning transmission electron microscopy (STEM) mode with a dispersion of 10 eV/channel in the 0–20 keV energy range. Detailed investigations of the phase structure and compositions were made in several spots along the interface between the Al 99.8 filler and the steel.

Results

Weld microstructure

A macroscopic view on the weld (Fig. 2a, scheme in Fig. 2b) shows the steel sheet, the Al-alloy sheet, and the Al 99.8 filler joining them. Obviously a weld has been established between the Al-alloy sheet and the Al 99.8 filler, while brazing has occurred between the steel sheet (which did not melt) and the filler. At the interface between the steel sheet and the Al 99.8 filler an intermetallic layer developed (Fig. 2c).

Brighter areas appear at both edges of the intermetallic layer in the backscattered electrons images of the overlapped joint (Fig. 3). EDX-analyses of these regions yield Zn and Al (Table 1). The Zn originates from the Zn coating of the steel sheet. At the edges of the interface between the Al 99.8 filler and the steel up to 60 at.% Zn is present in the filler (Fig. 3b, position indicated as '2'), which corresponds to the chemical composition of the eutectoidal fcc-Al + hcp-Zn [15]. In the zone adjacent to the edges the filler contains Zn dendrites in an Al matrix, having a hypoeutectoidal composition (Fig. 3b, position indicated as '1'). In regions near the interface to the steel (Fig. 3a) Zn is present on the grain boundaries of the Al 99.8 filler ([16–18] denominate this a cellular structure), further on up to 4 at.% Fe and a high porosity were detected (Fig. 3c).

Along the steel/Al interface the intermetallic layer shows a characteristic inhomogeneity in its thickness (Fig. 4). The interface between the intermetallic phase and the steel appears to be heavily serrated while the interface between the intermetallic phase and the Al 99.8 filler is comparatively smooth (serrations are smaller and more frequent). The mean thickness of the intermetallic layer is 2.3 ± 0.6 μm, its minimum thickness is 1.1 μm and its maximum thickness amounts to 4.2 μm.

In addition to the intermetallic phase seam along the steel/filler interface, in the filler Fe rich areas elongated perpendicular to the steel/filler interface are present (Fig. 4c). TEM–EDX analysis showed them to contain 19.5 ± 0.8 at.% Fe and <1 at.% Zn.

Structure, chemical composition and morphology of the intermetallic phases at the steel/Al 99.8 filler interface

TEM investigations reveal that the intermetallic layer at the steel/filler interface contains grains with different morphologies (Fig. 5). At the interface between the intermetallic layer and the Al 99.8 filler elliptical grains predominate, whose long axes usually are approximately perpendicular to the interface. In contrast, larger trapezoidal grains have formed at the interface to the steel. The interfaces between the trapezoidal grains and the surrounding phases appear straight on the steel side and wavy on the Al 99.8 filler side where

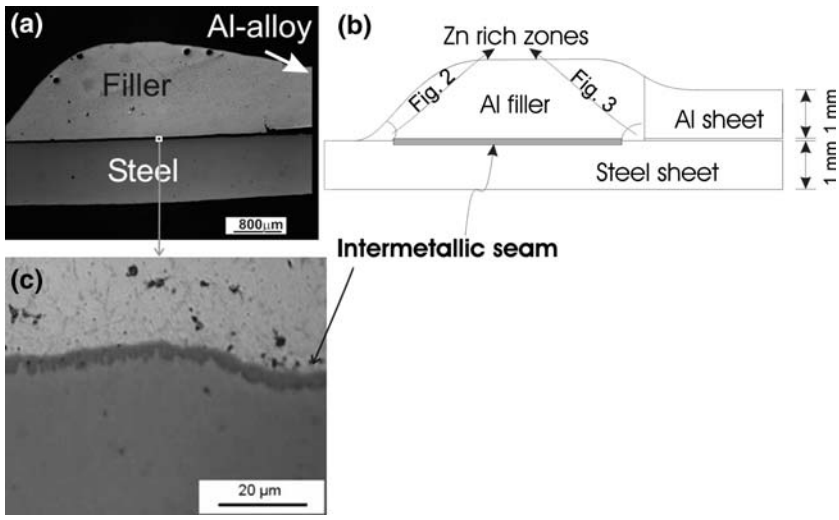

Fig. 2 (**a**) Macroscopic micrograph of the joint. (**b**) Scheme of the transverse view of the system showing the A6061 T4 and the steel sheets and the Al 99.8 filler. (**c**) Optical micrograph showing the intermetallic seam

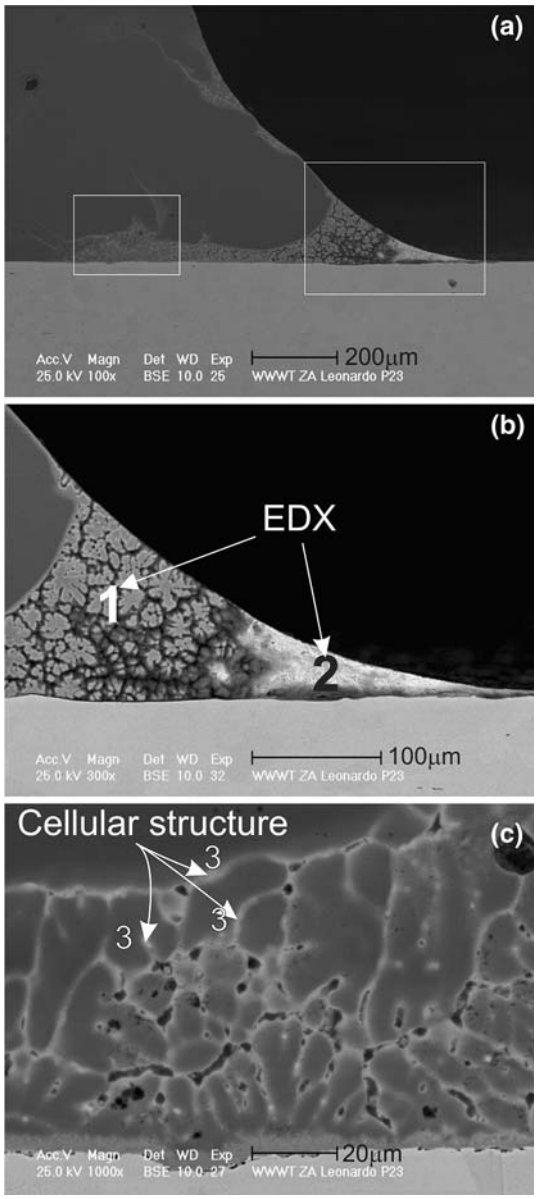

Fig. 3 (**a**) General view of the outer part of the steel/Al 99.8 filler interface. (**b**) Detail of (**a**) showing Zn–Al dendrites (*left*) and almost pure Zn (*right*). (**c**) detail of (**a**), where Zn is present at the grain boundaries of the filler

Table 1 EDX analysis of aluminium-zinc rich areas 1, 2 and 3 indicated in Fig. 3

	Al (at.%)	Zn (at.%)	Fe (at.%)
1	80 ± 2	20 ± 3	0
2	40 ± 4	59 ± 4	1 ± 0.5
3	82 ± 4	16 ± 3	3 ± 1

the elliptical grains are. The trapezoidal grains are separated by finger-like remains of the steel, which render the interface its characteristic serrated feature. The large trapezoidal grains at the interface to the steel appear substantially richer in Fe and poorer in Al than the elliptical grains at the interface to the Al in EDX analyses. However, due to the small differences in the Fe and Al content of the known Fe_xAl_y-phases [19], the phases present at the steel/filler interface had to be identified by their electron diffraction patterns. Electron diffraction patterns performed on the large trapezoidal grains confirm them to be the so-called η-phase (Fig. 6), a Fe_2Al_5 orthorhombic phase [20]. The elliptical grains between the Fe_2Al_5 grains and the Al 99.8 filler were identified as the so-called θ-phase (Fig. 7a, b), a $FeAl_3$ monoclinic phase [21]. EDX-analyses in the scanning transmission electron microscopy (STEM) mode revealed the composition of the $FeAl_3$ as 27 ± 3 at.% Fe and 73 ± 3 at.% Al, and the composition of Fe_2Al_5 as 30 ± 2 at.% Fe and 70 ± 2 at.% Al; the extreme values of the chemical composition measured defining the homogeneity range for the intermetallic phases $FeAl_3$ and the Fe_2Al_5 are shown in Table 2.

The $FeAl_3$ monoclinic phase (lattice constants: $a = 1.5489$ nm, $b = 0.8083$ nm, $c = 1.2476$ nm, $\beta = 107.70°$ [22]) detected adjacent to the Al 99.8 filler consists of elliptical grains with a long axis of 440 ± 180 nm and a short axis of 180 ± 64 nm. Their aspect ratio is 2.5 ± 0.8. TEM bright-field images and the overlapping of diffraction patterns reveal that often two or three $FeAl_3$ grains are superimposed on each other. Since the thickness of the foils used for the TEM investigations is roughly 200 nm, the thickness of the $FeAl_3$ crystals can be estimated to be in the order of a few ten nm. While the $FeAl_3$ grains directly adjacent to the Fe_2Al_5 grains appear mostly to have an elliptical shape (their long axis is perpendicular to the steel/Al 99.8 filler interface) other $FeAl_3$ grains, especially those who are not direct neighbours of Fe_2Al_5 grains have a discoidal rather than an elliptical shape. Both the elliptical and the discoidal grains of the $FeAl_3$ phase contain a high density of microtwin boundaries (Fig. 7c). These microtwins are visible in the bright field images, further on streaks appear in the diffraction patterns; no other crystal defect was detected. In the grain shown in Fig. 7 we determined the twin boundaries to be stacked on the (4–4–1) planes.

The morphology of the Fe_2Al_5 can be characterized by trapezoidal, faceted, single-crystals (Figs. 4–6, 8). These crystals are 1.7 ± 0.4 µm long and 1.1 ± 0.5 µm wide, their aspect ratio is about 1.5 ± 0.8. The crystal structure of Fe_2Al_5 is orthorhombic (lattice constants: $a = 0.7656$ nm, $b = 0.6415$ nm, $c = 0.4218$ nm [23]). In Fe_2Al_5, long individual dislocations and glissile dislocation half-loops can be observed (Fig. 8), which nucleate from the phase boundaries. They indicate that

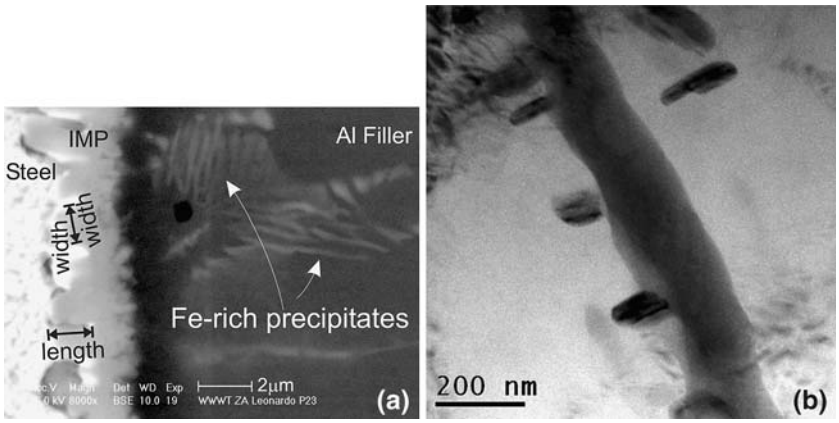

Fig. 4 (**a**) SEM micrograph in back scattered electrons mode, showing an overview of the morphological aspects at the IMP as well as the stripe-like phase formed in the aluminium filler near to it. (**b**) BF-TEM micrograph of an elongated arm of the Fe-rich precipitate and its surrounding smaller ellipsoidal precipitates

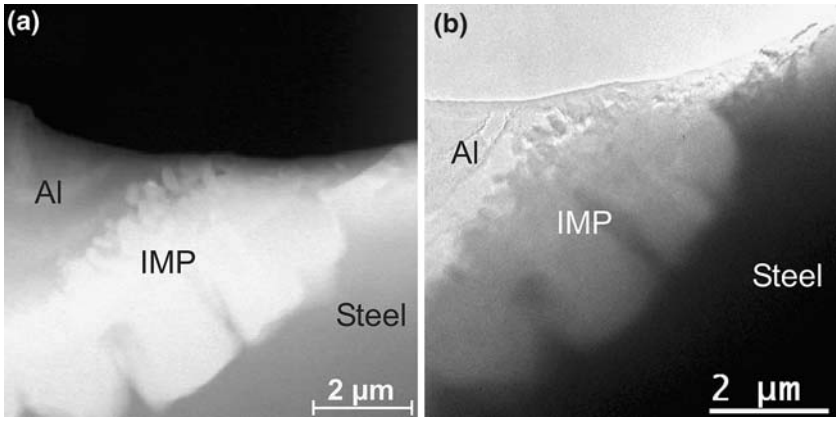

Fig. 5 Morphology of grains present at the IMP, resolved in: (**a**) STEM mode, (**b**) TEM-BF mode

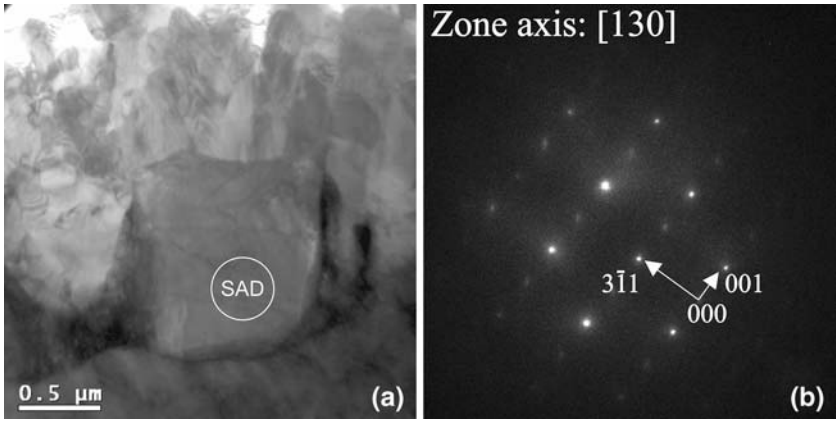

Fig. 6 (**a**) BF-TEM micrograph of a region of the IMP. (**b**) Indexed selected area diffraction (SAD) pattern corresponding to the region marked in (**a**), identifying this phase as Al_5Fe_2

Frank–Read sources were activated at the straight part of the interface between Fe_2Al_5 and the $FeAl_3$. In bright and dark field images of Fe_2Al_5 oscillation contrasts of lines appear (Fig. 8). In Ref. [21] a similar contrast, referred to as tweed patterns, was explained through a chemical modulation originated by partial occupation of positions 1 and 2 (occupancies of 0.32 and 0.24, respectively) of aluminium atoms in the crystal structure of Fe_2Al_5 [20], however, the pattern observed here might also be caused by Moiré fringes.

The finger-like areas in-between the Fe_2Al_5 grains are sharp triangles directed towards the interface, forming a small angle of $20 \pm 9°$ (Fig. 9a, d). EDX-analyses showed that the steel in these areas contains up to 20 at.% Al (Fig. 9b). Diffraction patterns (Fig. 9c) revealed that they are steel remains (α-Fe). The finger-like structures belong to larger steel grains, which surround the individual Fe_2Al_5 grains. Near the interface to the Fe_2Al_5 a high dislocation density was observed in the steel grains.

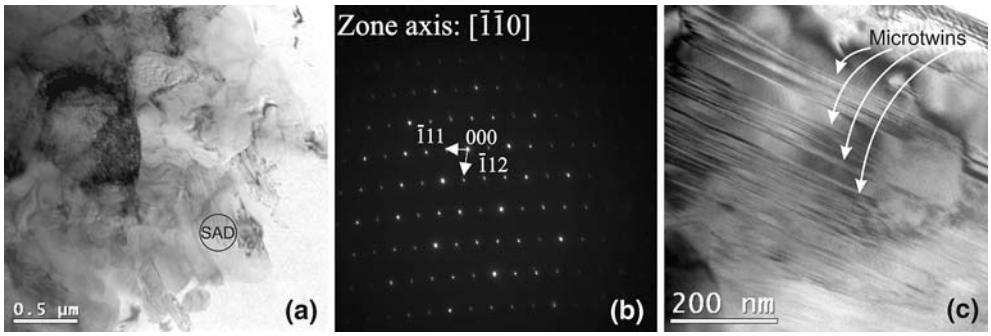

Fig. 7 (**a**) BF-TEM micrograph of an elliptical grain containing a high microtwinning density. (**b**) Indexed SAD pattern of the grain indicated in (**a**), identified to be Al_3Fe, in which the spots are slightly elongated as a consequence of the microtwins. (**c**) Magnified BF-TEM micrograph of an Al_3Fe grain highlighting microtwins

Table 2 Chemical homogeneity range determined by EDX analysis of phases Al_5Fe_2 and Al_3Fe

	Fe (at.%)	Al (at.%)	Al/Fe ratio
Al_5Fe_2			
Max	32	73	
Min	27	68	
Mean	30	70	2.4
±	2	2	0.2
Al_3Fe			
Max	32	78	
Min	22	68	
Mean	27	73	2.7
±	3	3	0.6

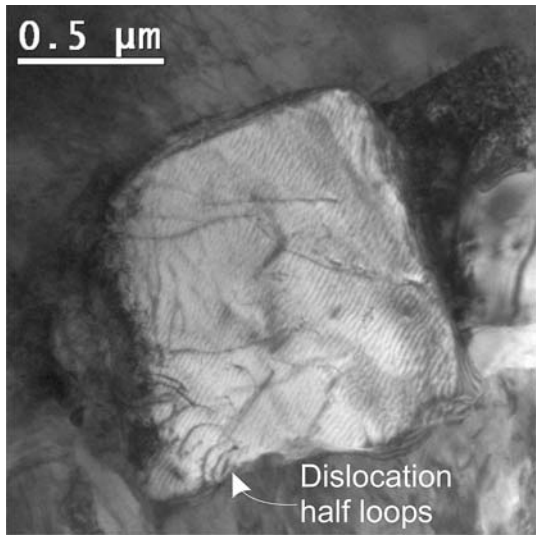

Fig. 8 BF-TEM micrograph of an Al_5Fe_2 showing Glissile dislocation half-loops

Discussion

Phases and phase morphologies in the intermetallic layer

In terms of the Fe–Al equilibrium diagram [1, 19] in the Al-rich corner the three phases $FeAl_3$ (θ-phase), Fe_2Al_5 (η-phase) and $FeAl_2$ (ζ-phase) and in the Fe-rich corner the phases FeAl and Fe_3Al might be expected to be present in the intermetallic phase layer. The $FeAl_3$, Fe_2Al_5, and $FeAl_2$ phases in the Al-rich corner do not differ strongly in their thermal stability and their chemical composition (the homogeneity ranges reported are 65.5–67 at.% Al for $FeAl_3$, 70–72.5 at.% Al for Fe_2Al_5 and 74.5–75.5 at.% Al for $FeAl_2$) [19]. Thus, in joints with layers of intermetallic phases as thin as those encountered here, only TEM diffraction patterns allow reliable phase identification. In accordance with earlier experimental investigations of intermetallic layers in the Fe–Al system [23–28] the TEM investigations performed here revealed that not all possible Fe_xAl_y phases are present, only Fe_2Al_5 and $FeAl_3$ were detected.

Intermetallic Fe–Al-layers formed in hot-dipping as well as in diffusion couples show a common characteristic morphology where polycrystalline $FeAl_3$ exists at the interface to the Al while tongue-like Fe_2Al_5 crystals extended into the steel [23, 25, 28]. In comparison to those intermetallic layers on hot-dip-aluminised steel, where the Fe_2Al_5 crystals usually have a length of several 10 μm to several 100 μm, in the steel/Al-alloy joints investigated here significantly thinner intermetallic layers have been formed due to the comparatively low temperatures and low heat loading of the CMT welding process. While in the intermetallic layers on hot–dipped steel and in diffusion couples the thickness of the Fe_2Al_5 sub-layer exceeds that of the $FeAl_3$ sub-layer by up to several orders of magnitude [27], in the joints investigated here the thickness of the Fe_2Al_5 sub-layer is of the same order of magnitude as the thickness of the $FeAl_3$ sub-layer. Compared to the studies of [26–28], where the

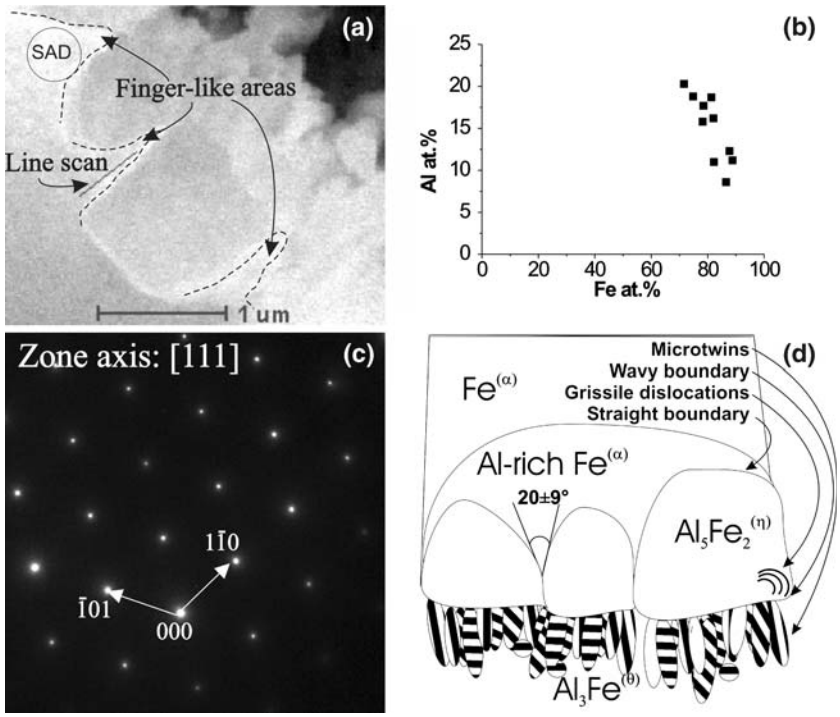

Fig. 9 (**a**) STEM micrograph of finger-like areas. (**b**) EDX elemental line scan of the finger-like area (marked in (**a**)). (**c**) Indexed SAD pattern (marked in (**a**)) revealing the finger-like areas to be $Fe_{(\alpha)}$. (**d**) Scheme of all the phases and their defects present at the IMP zone

Fe_2Al_5 phase is characterized by a tongue-line appearance, here the length to width ratio of the Fe_2Al_5 crystals is significantly smaller, the grains appear almost equiaxial. The tongue-like morphology of the Fe_2Al_5 phase in the sub-layers built in hot-dipping and in diffusion couples has been attributed to anisotropic diffusion. A particularly high diffusion rate in Fe_2Al_5 occurred in the direction of the longest axis of the orthorhombic crystal lattice where structural vacancies are present (the longest axis of the Fe_2Al_5 crystal structure is denominated as "*a*"-axis in the newer literature [20] while named "*c*"-axis in older publications [24]). This anisotropic diffusion accounts for a columnar growth of Fe_2Al_5 perpendicular to the Fe–Al-interface in diffusion couples [24, 25].

The almost equiaxial morphology of the Fe_2Al_5 and its similar thickness to the $FeAl_3$ shows, that contrary to the intermetallic layers reported so far, the intermetallic Fe_2Al_5 sub-layer investigated here did not grow predominately by diffusion along the longest crystallographic axis. Since the thickness of our intermetallic layers is only a few μm their main growth mechanism presumably is by chemical reaction as proposed by [27–29] for the early stage of intermetallic layer growth in hot-dipping.

Phase formation sequence and phase growth in the intermetallic layer

Predictions about the phase sequence in Fe–Al-intermetallics on the Al-rich side are equivocal. For solid metal-metal systems the Walser–Bené model [30] would predict $FeAl_3$ to be formed before Fe_2Al_5, while according to Pretorius' model [31, 32] of the effective heat of formation the Fe_2Al_5 would be formed first. Lee et al. [5] extended Pretorius' model towards sequences of intermetallic phases in liquid–solid systems by introducing an effective free energy of formation. The gist of this concept is that the phase with the lowest free energy of formation value at the composition of the lowest liquidus is formed first. This concept would predict $Al_{13}Fe_4$, a phase similar to Fe_3Al to be formed first. However, it appears doubtful whether the free energy at the composition of the lowest liquidus is relevant since here a phase is formed from the liquid Al and the solid Fe. It also might be expected that in case of temperatures exceeding the melting point of the Fe_2Al_5, the Fe_2Al_5 is formed first, having the lowest free energy in this temperature range.

Another indication that the Fe_2Al_5 is the phase formed first is its wavy interface towards the Fe_3Al, which indicates in a binary system that it was a former interface between a liquid and a solid, while the straight interface of the Fe_2Al_5 on the steel side indicates solid-state diffusion [33]. This is in good agreement with [26], where $FeAl_3$ was formed during solidification of Al after withdrawal of the steel from the Al bath (in hot-dipping tests) [26]. A further indication of the prior formation of the Fe_2Al_5 is the fact that each Fe_2Al_5 grain is a direct neighbour to several $FeAl_3$ grains, thus it appears likely that the $FeAl_3$

nucleated at the interface of the already formed Fe_2Al_5.

The large size and the low number of the Fe_2Al_5 single crystals imply a very limited number of nuclei. In contrast to previous investigations of intermetallic phases formed by hot-dipping and in diffusion couples, the longest axis of the orthorhombic Fe_2Al_5 single crystals does not point perpendicular to the interface, but it is inclined to the interface. Thus, contrary to e.g. [34, 35], not the orientation of the longest axis of the Fe_2Al_5 but rather the nucleation conditions, as already suggested by [26], are the cause for the serrated structure of the steel–Fe_2Al_5 interface. The inclination of the longest axis of the Fe_2Al_5 to the direction perpendicular to the steel/Al 99.8 filler interface is probably due to a superposition of the directions of the temperature gradient perpendicular to the steel/Al 99.8 filler interface and the temperature gradient caused by the forward motion of the filler in the welding process. The fact that the longest axis of the Fe_2Al_5 (where diffusion is high due to the large number of structural vacancies) is not perpendicular to the steel/Al interface presumably decreases the growth velocity of the Fe_2Al_5.

The $FeAl_3$ grown on the grain boundaries of the Al filler is due to diffusion of the Fe into the melt and a eutectic reaction during cooling; similar regions of $FeAl_3$ have also been detected at the interface in hot-dip aluminised steel [27, 38]. The strong increase of volume during the formation of the $FeAl_3$ [23] results in high stresses, which may be responsible for the high microtwin density found in the $FeAl_3$ grains and for the dislocations in the Fe_2Al_5 grains. The $FeAl_3$ does not show a strong preferential growth orientation, which is probably due to the fact that there is not one unique epitaxial relationship between $FeAl_3$ and Fe_2Al_5 [30, 37]. The high internal stresses formed due to the large volume increase during Fe_2Al_5 formation as well as the high cooling rates in the weld may be due to a large misfit between $FeAl_3$ and Fe_2Al_5. The low temperature of the weld pool and the cold surrounding material, that leads to rapid cooling, have prevented the disintegration of $FeAl_3$ in favour of Fe_2Al_5 and thus, pore formation at the interface between $FeAl_3$ was not observed, although it occurred e.g. in diffusion couples [24] and TIG welds [39].

In the Al-filler near the interface to the $FeAl_3$ high Fe concentrations appeared due to Fe diffusion into the melt, however during cooling an oversaturation of the melt occurred resulting in the precipitation of a Fe rich intermetallic phase [40]. The precipitates have a fir-tree like morphology (Fig. 4), which is supposedly due to temperature oscillations [41]. The CMT process presumably induces temperature oscillations by the periodic dipping of the filler into the melt and its subsequent extraction. Oscillations in the uniformity of the melt could also be induced by the periodical fall of the drops as the tip of the electrode withdraws from the melted pool.

Role of the Zn coating for the phase formation in the intermetallic layer

Microscopy revealed that the Zn in the joint has been driven away from the steel surface towards the steel–filler interface outer boundary of the joint as well as to the steel/filler/Al-alloy sheet interface at its inner boundary. The Zn is known to improve the wetting of Fe by Al-alloy melts [29, 42]. Compared to Fe, Al has a larger affinity to Zn, thus usually intermetallic Al–Zn-phases are favoured compared to the intermetallic Fe–Zn phases [29, 43]. While $Fe_2Al_5Zn_x$ with up to 23 wt.% Zn has been observed earlier [44, 45] no significant Zn enrichment of the Fe_2Al_5-phase was found in this weld. Similarly to [8, 25] here a direct contact between the Al and the Fe occurred despite the Zn coating of the steel.

The regions with high Zn content at the outer and inner boundaries resemble partly rapidly solidified [46–49] Al–Zn-alloys, which contain Zn-rich dendrites. In adjacent regions with lower Zn content the Zn appears at the grain boundaries of the Al and often pores are visible at triple points. The origin of these pores might be explained either by the escape of the inert gas during the process out of the molten Al filler or by the formation of gas bubbles in the Al filler as a result of its decrease in solubility as it solidifies and cools down. Due to the high fluidity of the molten Zn, which reaches temperatures much higher than its melting point, it may have been transported by the outgoing gas towards the edges of the plates and the filler. Given the fact that Zn reactions with the steel are oppressed under the presence of Al, the Zn tends to escape, following a capillary effect, through the cavity between the steel plate and the Al filler respectively Al sheet forced to be joined. Once the Zn gets into contact with the cold atmosphere, it rapidly solidifies. Therefore, the Zn concentration decreases from the edges of the filler/steel plate interface, as well as from the contact Al plate/filler/steel, into the filler. Depending on their concentration and cooling rate, the Zn rich zones adopt different morphologies: thin cellular structures at the inner Zn containing part, a fine eutectoidal structure at the outermost part of the interface filler/steel and thick dendrites in-between the latter two zones [46–49].

Conclusions

We studied steel/Al-alloy joints manufactured by the CMT-joining method developed by Fronius GmbH. The joint is characterized by a weld between the Al-sheet and an Al 99.8 filler material and a brazing of the Al 99.8 filler to the steel sheet.

The zinc coating of the steel sheet improved the wetting of the steel in the centre of the overlap joint. At the outermost part of the edges of the joint Al–Zn eutectic and areas with hypoeutectic Al–Zn compositions were obtained, and beside these areas zinc diffused in the grain boundaries of the Al 99.8 filler.

At the interface between the steel and the Al 99.8 filler two intermetallic phases, Fe_2Al_5 and $FeAl_3$ were formed. The thickness of the intermetallic phase seam is about 2.3 μm, which is significantly thinner than similar intermetallic phase seams obtained by other joining processes dealing with the same system. The Fe_2Al_5 is characterized by trapezoidal, nearly equiaxial single grains surrounded by Al rich remains of the steel grains. The growth direction of the Fe_2Al_5 crystals does not correlate with their longest crystal axis. The $FeAl_3$ grains are significantly smaller than the Fe_2Al_5 grains and most often elliptically shaped. The longest axis of the ellipsoids is nearly perpendicular to the original interface between the steel and the Al 99.8 filler. Most of the $FeAl_3$ grains contain a large amount of microtwins, which are presumably due to high stress caused by the volume expansion associated with the formation of the $FeAl_3$ phase.

In the region near the intermetallic phase seam the Al 99.8 filler contains iron rich precipitates, which are presumably due to the diffusion of iron into the filler and precipitation from the oversaturated melt.

Acknowledgements Financial support from the Hochschuljubiläumsstiftung der Stadt Wien (grant (H-175/2001) is gratefully acknowledged by one of the authors (D Eyidi). Further we wish to thank A Leitner, voestalpine Stahl GmbH and R Rechberger, voestalpine mechatronics GmbH for the preparation of the samples.

References

1. Kattner UR (1990) In: Binary alloy phase diagrams. ASM International, Materials Park, OH, USA
2. Iwamoto N, Yoshida M, Tabata S, Takeuchi T, Makino M (1975) Trans JWRI 4:67
3. Rathod MJ, Kutsuna M (2004) Weld Joining 16S
4. Hartwig H (1981) Aluminium 57:615
5. Lee WB, Yeon YM, Kim DU, Jung SB (2003) Mater Sci Technol 19:773
6. Fukumoto S, Tsubakino H, Okita K, Aritoshi M, Tomita T (2000) Scr Mater 42:807
7. Kobayashi A, Machida M, Hukaya S, Suzuki M (2003) JSME Int J Ser A 46:452
8. Bel'chuk GA (1963) Svar Proizvod 11:3
9. Bach FW, Möhwald K, Holländer U, Duda T (2003) DVS-Schriftenreihe 212:231
10. Kreimeyer M, Wagner F, Vollertsen F (2003) In: Propawe R (ed) Proceedings of the 2nd international WLT-conference on lasers in manufacturing, Munich, June 2003. AT-Fachverlag, Stuttgart, p 235
11. Pinto H, Pyzalla A, Hackl H, Bruckner J (2006) Mater Sci Forum 524–525:627
12. Schmaranzer CH (2004) In: Herstellung, Mikrostruktur und Eigenschaften von Stahl-Aluminium Hybridplatinen. Dissertation, TU Vienna, Austria, p 243
13. Bruckner J, Wagner J, Arenholz E (2005) In: Kaufmann H (ed) Proceedings of the 2nd international light weight metals technology conference 2005. LKR-Verlag, Austria, p 275
14. Stadelman PA, Buffat PA (1987) Ultramicroscopy 21:131
15. Murray JL (1986) In: Massalski TB (ed) Binary alloy phase diagrams. ASM International, Materials Park, OH, p 185
16. Watkins KG, McMahon MA, Steen WM (1997) Mater Sci Eng A 231:55
17. Da Rocha OFL, Siqueira CA, Garcia A (2002) Mater Res (London) 5:391
18. Lin X, Huang W, Feng J, Li T, Zhou Y (1999) Acta Mater 47:3271
19. Kubaschewski O (1982) Iron–binary phase diagrams. Springer-Verlag, Berlin, p 5, 185
20. Burkhardt U, Grin Yu, Ellner M (1994) Acta Crystallogr Sect B Struct Sci 50:313
21. Griger A, Stefaniay V, Turmezey T (1986) Z Metallkunde 77:30
22. Black PJ (1955) Acta Crystallogr 8:43
23. Gebhardt E, Obrowski W (1953) Z Metallkunde 44:154
24. Heumann T, Dittrich S (1959) Z Metallkunde 50:617
25. Andrews DR (1964) Sheet Met Ind 933
26. Eggeler G, Auer W, Kaesche H (1986) Z Metallkunde 77:239
27. Bouché K, Barbier F, Coulet A (1998) Mater Sci Eng A 249:167
28. Bouayad A, Gerometta Ch, Belkebir A, Ambari A (2003) Mater Sci Eng A 363:53
29. Marder AR (2000) Prog Mater Sci 45:191
30. Walser RM, Bené RW (1982) Appl Phys Lett 41:529
31. Pretorius R, Vredenberg AM, Saris FW, de Reus R (1991) J Appl Phys 70:3636
32. Theron CC, Ndwandwe OM, Lombaard JC, Pretorius R (1996) Mater Chem Phys 46:238
33. Bouché K (1995) Etude Thermocinétique de la Dissolution de Métaux Solides (Fer et Nickel) Dans L'Al Liquide. PhD thesis, Universite de Provence, p 194
34. Richards RW, Jones RD, Clements PD, Clarke H (1994) Int Mater Rev 39:191
35. Kwon SC, Lee JY (1981) Can Metall Q 20:154
36. Guttmann M (1994) Mater Sci Forum 155–156:527
37. Gösele U, Tu KN, Thompson RD (1982) J Appl Phys 53:8759
38. Eggeler G, Vogel H, Friedrich J, Kaesche H (1985) Pract Metallogr 22:163
39. Ryabov VR, Duplyak VD (1965) Svar Proizvod 2:42
40. Ahravci CA, Pekgüleryüz MÖ (1998) Calphad 22:147
41. Triverdi R, Park JS (2002) J Cryst Growth 235:572
42. Bluni ST, Notis MR, Marder AR (1995) Acta Metall Mater 43:1775

43. Kato T, Nunome K, Kaneko K, Saka H (2000) Acta Mater 48:2257
44. Tang NY (2000) J Phase Equilib 21:70
45. Perrot P, Tissier JC, Dauphin JY (1992) Z Metallkunde 83:786
46. Ceylan M, Akoy I, Kuzucu V, Balo S (1997) J Mater Process Technol 65:41
47. Lin X, Huang W, Feng J, Li T, Zhou Y (1999) Acta Mater 47:3271
48. Feng J, Huang WD, Lin X, Pan QY, Li T, Zhou YH (1999) J Cryst Growth 197:393
49. Zhu YH, Man HC, Lee WB (2003) J Mater Process Technol 139:296